Appl. Phys. B 64, 429–433 (1997)

Applied Physics B Lasers and Optics

Generation and intrinsic dynamics of ring dark solitary waves

D. Neshev[1], A. Dreischuh[1], V. Kamenov[1], I. Stefanov[1], S. Dinev[1], W. Fließer[2], L. Windholz[2]

[1] Sofia University, Department of Quantum Electronics, 5, J. Bourchier Blvd., BG-1164 Sofia, Bulgaria
(Fax: + 359-2/962 5276, E-mail: aldrei@phys.uni-sofia.bg)
[2] Technische Universität Graz, Institut für Experimentalphysik, Petersgasse 16, A-8010 Graz, Austria
(Fax: + 43-316/873 8655, E-mail: windholz@fexphds01.tu-graz.ac.at)

Received: 24 June 1996

Abstract. We present experimental results on the evolution of ring dark solitary waves generated by computer-synthesized holograms. The data obtained and the detailed comparative numerical simulations show that this approach ensures reproduction of the correct intensity and phase portrait of the dark wave at the entrance of the nonlinear medium. The transverse dynamics at both even and odd initial conditions is studied and compared with the theory and simulations.

PACS: 42.65.S, 42.40.J, 42.65.J

The Ring Dark Solitary Waves (RDSW) in bulk nonlinear media are first introduced and described in the adiabatic approximation of the soliton theory in the works of Kivshar and Yang [1, 2]. In each diametrical slice of the background beam, the dark formation appears in the form of two intensity dips of hyperbolic-tangent profiles spaced at twice the dark ring radius. The phase portrait of the RDSW demonstrates pairs of abrupt π-phase shifts localized at the intensity minima across the ring. Similar to the one-dimensional and quasi-2D experiments described in [3, 4], in the first experimental generation of RDSWs [5] at a pure amplitude modulation at the entrance of the nonlinear medium, pairs of diametrical phase-shifts (less than π) within the dark ring are recorded [6]. The transverse velocity of these 2D dark formations of ring symmetry was found [5] to exceed the velocity of the 1D gray soliton stripes generated from even initial conditions (i.e. at pure amplitude modulation). In view of the principle possibility multiple signal beams to be guided parallely by RDSWs [7], the improvement of their contrast and the reduction of their transverse velocity is desirable. The same seems to be valid also for the ring-shaped bright solitons with topological charge introduced recently [8].

In this work, we present experimental data on the amplitude and phase distribution across ring dark formations obtained by reproducing computer-generated holograms, which ensure the adequate initial conditions for the generation of RDSWs of an improved contrast. It was found both experimentally and numerically that this RDSWs does obey weaker transverse dynamics as compared to the gray RDSW obtained at an initial pure amplitude modulation. Further reduction of the transverse velocity was reached by increasing the dark ring radius with respect to its width.

1 Computer-generated holograms and reconstruction analysis

Computer-Generated Holograms (CGH) have been used [9–11] to ensure the required intensity and spiral-phase distribution [12] of optical vortex solitons. The desired CGH of an odd dark wave of a circular symmetry should result from an interference between a reference plane wave $I_R(x, y)$ incident at the certain angle θ with respect to an object wave $I_D(x, y) \propto |E_D(r, \varphi)|^2$. In the object wave the dark ring of radius R_0 and width r_0

$$E_D(r, \varphi) = B(r)\tanh[(r - R_0)/r_0]\exp\{i\phi\} \tag{1a}$$

should be imposed on a background beam $B(r)$. In the above notations φ is the azimuthal coordinate ($\varphi \in [0, 2\pi]$), $r = (x^2 + y^2)^{1/2}$, and

$$\Phi(r) = \begin{cases} -\pi/2 & \text{for } r \le R_0, \\ +\pi/2 & \text{for } r > R_0 \end{cases} \tag{1b}$$

represents the diametrical phase jump across the ring dark formation. It is known that only the π-phase jump at the entrance of the Nonlinear Medium (NLM) is able to form a fundamental 1D dark soliton stripe (grid) [4]. This result encouraged us to synthesize CGHs by pure phase modulation of the object wave.

The interference pattern obtained by using the well-known relation

$$I(x, y) = I_R(x, y) + I_D(x, y) + 2\sqrt{I_R(x, y)\ I_D(x, y)} \times \cos\left(\frac{2\pi}{\lambda}\, x\, \cos\theta + \Phi\right) \tag{2}$$

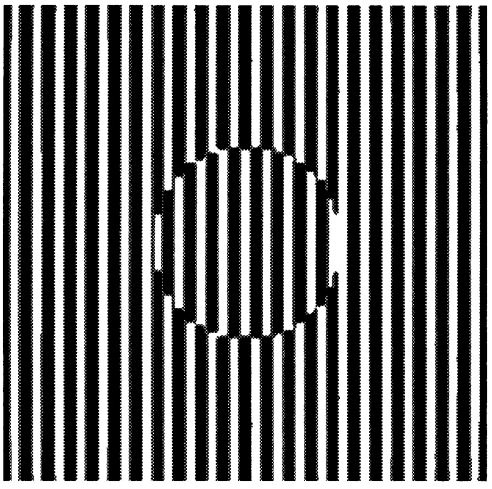

Fig. 1. Computer-generated hologram of a ring dark formation obtained at a pure π-phase modulation in the object beam

is shown in Fig. 1. The spatial position of the circular π-phase jump can be easily identified by the shift of the interference lines in the central region. During the numerical generation and reconstruction of the holograms of this type with variable ring-radii R_0 an 1024×1024 grid-mesh was used. The real CGHs, however, were produced photolitographically at a grating period of 20 μm on $15 \times 15\ \text{mm}^2$ optical glass substrates.

Following the classification of the types of CGHs [13], the discussed ones are of binary transmittance. At equal widths of the transmissive and reflective stripes (Fig. 1) it is shown analytically [13] that the even diffraction orders (except this with $m = 0$) should disappear. In our case, the diffraction efficiency at first orders was estimated to be 8.5%, close to the 10% limit predicted [13], whereas the diffraction efficiency in the even orders was negligible (Fig. 2a). Fig. 2b, c demonstrate two ring dark formations of different radii reconstructed from CGHs (in the $\pm$ 1-st diffraction orders) and the zero-order transmitted beam. Since the interference structure was quantized in two discrete levels, an irreducible quantization noise is added to the reconstructed wavefronts. According to [13], however, the mean square error is down to $\pi/24$.

In the first step of the CGH reconstruction analysis, we measured the transverse phase shift of the ring dark formation generated. Interference was obtained in a Mach–Zehnder interferometer (Fig. 3) formed by a beam splitter BS1, the mirrors M2 and M4 and the beam splitter cubes C1 and C2. For a purpose of a controllable optical path-length variation, a Michelson interferometer (BS2, M3, M4) was built-in in its reference arm. The path-length was changed by the piezoceramic transducer mounted mirror M4 and sensed by the variations in the interference pattern in the Michelson interferometer via the photodetector D. The telescope T2 was used to expand the He–Ne laser beam over the hole aperture of the CGH, whereas the iris-diaphragm ID placed 15 cm behind transmitted only the first diffraction-order beam with the reconstructed dark formation nested in. The telescope T1 was used to adjust the spatial frequency of the interference

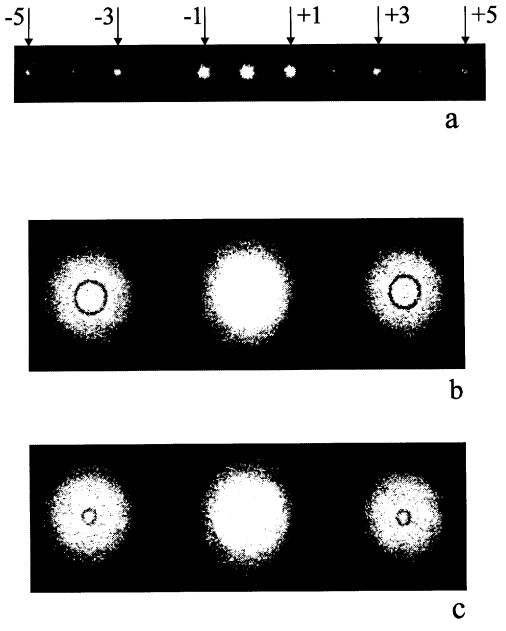

Fig. 2. Overview CCD camera images of some of the diffraction orders **a**) and zero and $\pm$ 1-st diffraction orders of two ring dark formations **b**, **c**) of different radii reconstructed from different Computer-Generating Holograms (CGHs)

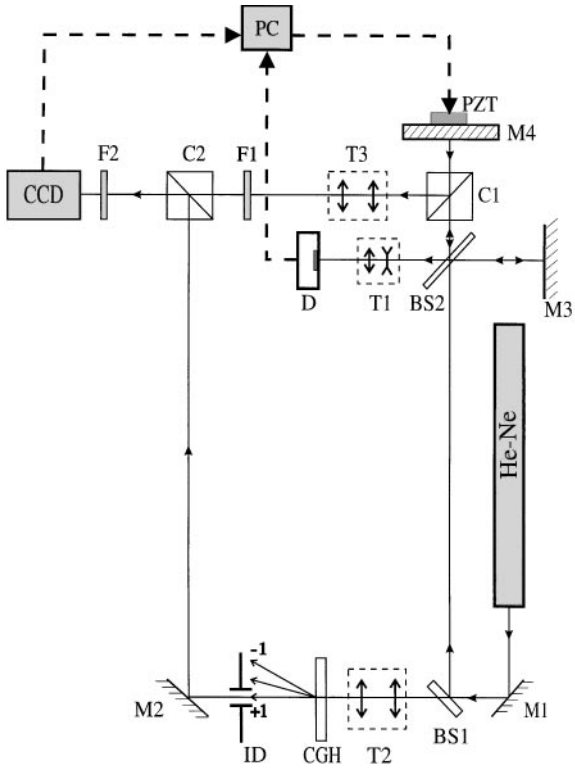

Fig. 3. Experimental setup used in the phase measurements (M1, M2, M3-mirrors; M4 and PZT-piezoceramic mounted mirror; BS1, BS2 – beam-splitters; T1, T2, T3-telescopes; C1, C2 – beam-splitter cubes; D – detector; F1, F2 – filter sets; CGH – computer generated hologram; ID – iris diaphragm; PC – personal computer; CCD – camera)

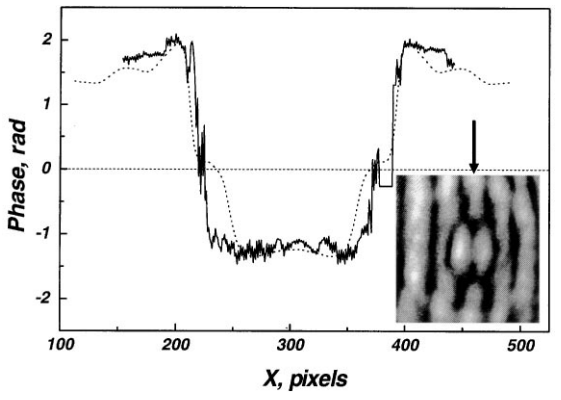

Fig. 4. Diametrical phase distribution of a ring dark formation reconstructed from CGH (solid line). **Dotted line** – numerical result obtained at $z = 45\ L_{\mathrm{Diff}}$ and $R_0/r_0 = 14$. **Insert** – Grayscale image of one of the interference patterns used in the tree-frame method for phase distribution retrieval

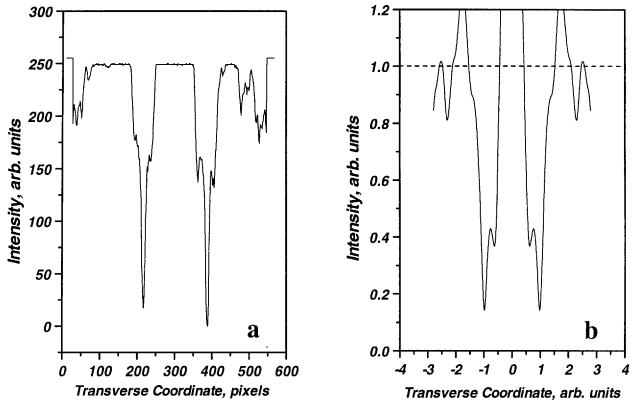

Fig. 5. Measured **a**) and simulated **b**) diametrical intensity distribution across the ring dark formation after a linear propagation over $z = 45\ L_{\mathrm{Diff}}$. (255 grayscale levels of the CCD array signal correspond to the initial background intensity)

pattern at the detector plane, whereas the telescope T3 matched the reference and object beam cross-section. Two filter sets F1 and F2 were used to avoid CCD-camera saturation at a direct CCD-array illumination and to control the interference pattern contrast. This arrangement has made possible to record sets of three interference pictures at known phase shifts $(0, 2\pi/3, 4\pi/3)$ per exposure and, thereafter, to reconstruct the 2D phase portrait of the dark formation by the three-frame technique [14, 6].

In Fig. 4 we present the experimental phase distribution across a dark ring of 2 mm diameter reconstructed form the CGH located 175 cm away from the CCD camera. The grayscale image inserted shows the system of interference lines used in this measurement. The arrow indicates the direction, at which the phase distribution evaluated is presented. Pairs of opposite phase shifts of nearly π are clearly seen. In a small region in the right wing of the curve, the phase was not adequately reconstructed because of the absence of intensity modulation in two of the frames recorded. Nevertheless, one can see weak distortions in the abrupt phase changes at the phase level denoted as zero and at the bottom of the phase step. We attributed these deviations to a diffraction of the dark ring.

The linear 2D evolution (diffraction) of optical beams along their propagation path could be described in a natural way by solving the $(2 + 1)$-dimensional nonlinear Schrödinger equation (NLSE) [1, 2]

$$\mathrm{i}\frac{\partial E_{\mathrm{D}}}{\partial z} + \beta\left(\frac{\partial^2}{\partial x^2} + \frac{\partial^2}{\partial y^2}\right)E_{\mathrm{D}} + kn_2|E_{\mathrm{D}}|^2E_{\mathrm{D}} = 0\,, \tag{3}$$

at $n_2 = 0$.

In (3) the term comprising $\beta = (2k)^{-1}$ accounts for the beam diffraction and $n_2|E_{\mathrm{D}}|^2$ is the medium refractive-index correction due to the presence of the intense beam inside the NLM (if present). In the linear reconstruction analyses (at $n_2 = 0$) (3) was solved numerically over 1024×1024 grid points. Closest agreement between the experimental (Fig. 4, solid line) and numerical results (dotted line) was found at $z = 45L_{\mathrm{Diff}}$ for $R_0/r_0 = 14$, where $L_{\mathrm{Diff}} = kr_0^2$ is the Rayleigh diffraction length. The result indicates that the phase variations at the half-high of the jump and at the phase-minimum results from the unavoidable diffraction. This was confirmed by placing the CGH 60 cm in front of the CCD camera. At this location the agreement between the experimental and numerical data was gradually better.

The ratio of the dark ring radius R_0 to the ring width r_0 deduced from the phase measurement and from the simulation agrees with the ratio measured directly by blocking the reference beam in the interferometer. For obtaining realistic profile of the intensity dip, we allowed saturation of the CCD camera (Fig. 5a). As seen from this slightly saturated experimental curve, recorded at 175 cm CCD-CGH distance, sufficiently longer than the 15 cm required for the CGH reconstruction, the 2D diffraction does influence also the dark ring intensity distribution. Assuming an initial hyperbolic-tangent profile of the dark beam (1) and a super-Gaussian background beam of a radius 5 times larger than R_0 the numerical simulation of the initial distribution at $z = 45L_{\mathrm{Diff}}$ and $R_0/r_0 = 14$ (Fig. 5b) was found to show the similar fine modulation to the observed experimental curve (Fig. 5a). The "saturation level" in the calculation is indicated in Fig. 5b with a dashed line.

Two particular conclusions could be drawn from the CGH reconstruction and from the simulations: i) at suitable distances the binary transmittance holograms generated at a pure phase modulation reproduce the π-phase jump encoded; ii) the intensity modulation of the dark ring is adequately described by hyperbolic-tangent profile.

Therefore we believe that it is possible to provide experimentally the conditions for the generation of ring dark solitary waves in self-defocusing nonlinear media (i.e. at $n_2 < 0$) [1, 2]

2 Transverse dynamics of RDSWs

The experimental arrangement for measuring the evolution of RDSWs radius R_0 and width r_0 along the nonlinear

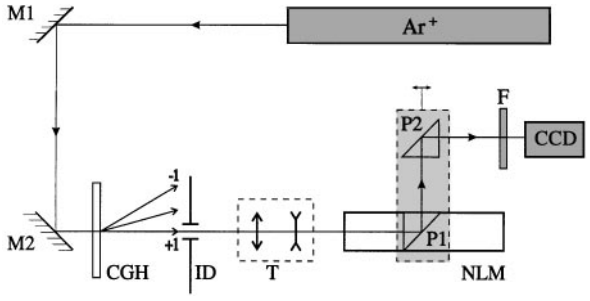

Fig. 6. Experimental set-up used for measuring the RDSW dynamics (Ar^+ – argon ion laser; M1, M2 – mirrors; CGH – computer generated hologram; ID – iris diaphragm; T – inverted telescope; NLM – nonlinear medium; P1, P2 – 90° prisms on a translation stage; F – filter set; CCD – camera)

propagation path is shown on Fig. 6. The 514.5 nm line of a multiline Ar ion laser of a power of 300 mW was used to reconstruct the CGH and the diameter of the first diffraction order beam at the entrance of the NLM of length 5 cm was reduced to 200 μm by a telescope. A pair of two identical prisms, one of them immersed in the nonlinear liquid (hydrocarbon oil 'Nujol'-Merck, dyed with $SPC_{16}6(NO_2)$ to a molar concentration of 1.1×10^{-3} Mol) provides the possibility to couple the background beam and the RDSWs out of the cuvette at variable lengths of the nonlinear propagation path. Under this conditions, the maximum nonlinear propagation length inside the cuvette was limited to 3.2 cm and the maximum nonlinear refractive-index change was $|\Delta n^{\mathrm{NL}}_{\max}| = 4.10^{-4}$. The eventual saturation of the CCD camera located at 21 cm after the exit of the NLM was prevented by suitable filter sets F (Fig. 6).

All further numerical simulations in this work are based on solving the NLSE (3) by the split-step Fourier method over 1024×1024 grid points under self-defocusing conditions ($n_2 < 0$) . The initially "black" RDSW at the entrance of the NLM was modelled according to (1a–b). In the nonlinear medium the longitudinal coordinate z was naturally to be expressed in units of nonlinear lengths $L_{\mathrm{NL}} = (k|n_2|A_0^2)^{-1}$, where A_0 is the amplitude of the background beam $B(r)$.

As a first step, we compared the transverse dynamics of "black" and "gray" RDSWs, the last one generated from initially even conditions

$$E_{\mathrm{G}}(r, \varphi, z = 0) = B(r) \tanh(r/r_0), \tag{4}$$

where $B(r)$ is the super-Gaussian background beam. The increase in the dark formation radius R_0 along the NLM is plotted in Fig. 7 for both initially "black" (solid line) and "gray" (dashed line) RDSWs. In order to ensure equal ring radii $R_0(z = 0)$ and widths $r_0(z = 0)$ in both cases, first the formation of the "gray" RDSW from pure amplitude modulation is simulated and, thereafter, the initial profile of the "black" RDSW was generated. Since the experimental conditions required imaging of the photolitographycally produced amplitude mask (reflecting dot) on the cuvette input face, initial diffraction over $3L_{\mathrm{Diff}}$ was included prior to starting solving the NLSE. As seen

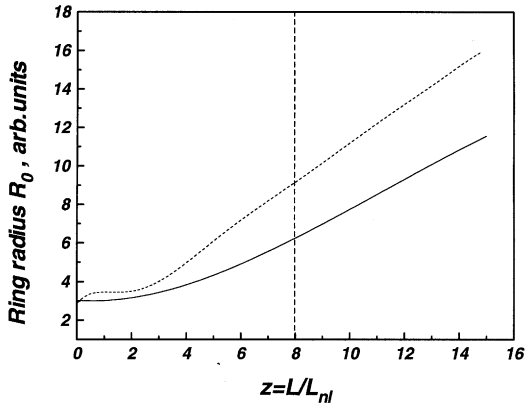

Fig. 7. Evolution of the Ring Dark Solitary Wave (RDSW) radius vs nonlinear propagation-path length in units of L_{NL} (solid line – initially "black" RDSW; dashed –"gray" RDSW generated from an even initial condition) The vertical line indicates the length, up to which the numerical data could be compared to the experimental ones in Fig. 8

from the numerical results (Fig. 7), the "black" RDSW radius does increase slower as compared to the radius of the "gray" formation generated by a pure amplitude modulation.

Qualitatively the same behaviour was found in the experimental results presented in Fig. 8. Since $L_{\mathrm{NL}} = L_{\mathrm{Diff}}$ in the simulation in Fig. 7 and $L_{\mathrm{Diff}} \approx 4$ mm in the NLM (due to the presence of telescope T in Fig. 6) the vertical dashed line in Fig. 7 indicates approximately the NLM length, up to which the data available from the experiment are comparable to the numerical results. Again it is evident, that the initially "black" RDSW reconstructed from the CGH (Fig. 8, closed triangles) does obey a reduced transverse dynamics as compared to the initial "gray" RDSW (open circles). The inclusion of the initial diffraction in the model seems to describe adequately the initial stage of the "gray" RDSW evolution (Figs. 7, 8, dashed curves), but does not further influence the transverse velocity of these "gray" formations.

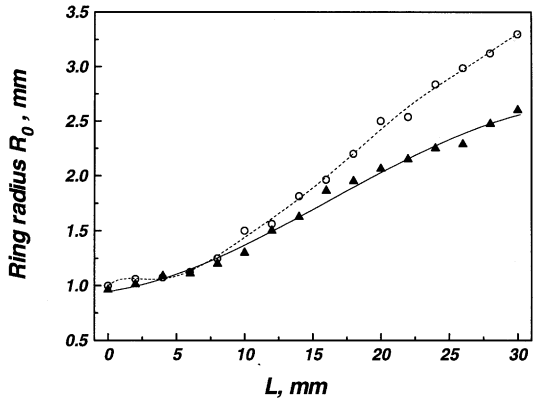

Fig. 8. Experimental dependence on the RDSW radius along the nonlinear medium (triangles – RDSW generated from a CGH; rings – RDSW generated by an amplitude mask) and corresponding fits

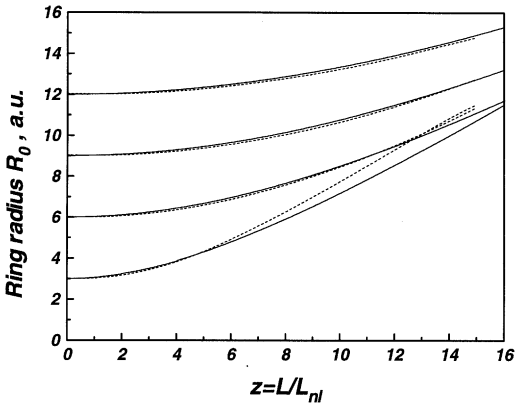

Fig. 9. RDSW radius R_0 vs normalized nonlinear propagation distance z at different values of $R_0/r_0|_{z=0}$ (solid curves – analytical results following [1], dashed – numerical solutions of the nonlinear Schrödinger equation)

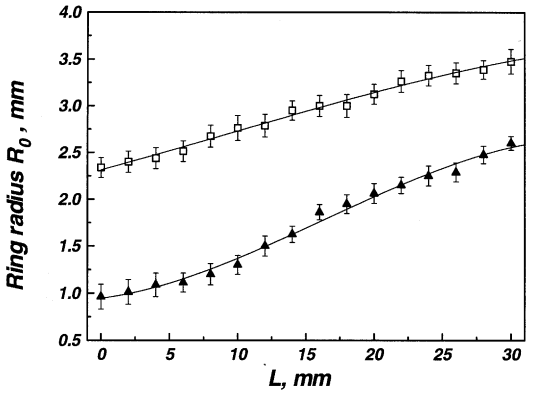

Fig. 10. RDSW radius R_0 measured at the CCD-camera plane vs nonlinear propagation path length L at $R_0(z=0)=12.5$ μm (**lower curve**) and $R_0(z=0)=85$ μm (**upper curve**) at the entrance of nonlinear medium. The bars indicate the measured values of the ring width r_0

As a second step we analysed both numerically and experimentally the dynamics of RDSWs of equal widths r_0 and different radii R_0, generated with odd initial conditions. Fig. 9 presents numerical results intended to clarify as far the analytical results on the RDSW radius R_0 vs z obtained in [1] match the solution of the NLSE. The radial spreading of the initially black RDSWs obviously is faster for dark odd rings of reduced radii R_0. The adiabatic approximation used in [1] is found to gradually influence the small rings only, whereas at $R_0 > 6r_0$ the numerical results (dashed curves) are practically identical to the analytical ones (solid curves).

The experimental results on the evolution of RDSWs obtained with CGHs (Fig. 10) confirm that the larger initially R_0 is, the weaker is the expressed dynamics of the dark formation along the NLM. The bars in Fig. 10 present the measured ring-widths r_0 along the propagation path. The decrease of the width r_0 in the RDSW with the smaller radius and the weak change of the curvature of the dependence are results of both the higher transverse velocity of this formation inside the NLM, and the diffraction from the side-lying exit of the cuvette to the CCD camera.

3 Conclusion

In view of the above analyses we are convinced to state that the reproduction of computer-generated holograms of binary transmittance generated at a pure phase modulation of the object wave are able to ensure adequate intensity and phase distributions for the generation of initially black ring dark solitary waves. These dark formations show a reduced dynamics as compared to the RDSWs generated by an amplitude modulation of the background beam. Further decrease of their transverse velocity is reached by increasing the RDSW radii.

Acknowledgements. The Bulgarian co-authors would like to thank the Technical University Graz, Institute of Experimental Physics, for the warm hospitality during their research stays. D.N. and V.K. were BMWFK-fellows. A.D. was a fellow of the Österreichischer Akademischer Austauschdienst. This work was supported partially by the CEEPUS-project (Network A-21) and by the National Science Foundation, Bulgaria.

References

1. Yu. Kivshar, X. Yang: Phys. Rev. **E50**, R40 (1994)
2. Yu. Kivshar, X. Yang: Chaos, Solitons and Fractals **4**, (1994)
3. D. Andersen, D. Hooton, G. Swartzlander, Jr., A. Kaplan: Opt. Lett. **15**, 783 (1990)
4. G. Swartzlander, Jr., D. Andersen, J. Regan, H. Yin, A. Kaplan: Phys. Rev. Lett. **66**, 1583 (1991)
5. S. Balushev, A. Dreischuh, I. Velchev, S. Dinev, O. Marazov: Appl. Phys. **B61**, 121 (1995); ibid., Phys. Rev. **E52**, 5517 (1995)
6. A. Dreischuh, I. Velchev, W. Fließer, S. Dinev, L. Windholz: Appl. Phys. **B62**, 139 (1996)
7. A. Dreischuh, V. Kamenov, S. Dinev: Appl. Phys. **B 63**, 145 (1996)
8. V. Afanasjev: Phys. Rev. **E52**, 3153 (1995)
9. N. Hekenberg, R. Mc Duff, C. Smith, A. White: Opt. Lett. **17**, 221 (1992)
10. S. Roux: Appl. Opt. **32**, 4191 (1993)
11. B. Luther-Davies: Opt. Lett. **15**, 1816 (1994)
12. M. Beijersbergen, R. Coerwinkel, M. Kristensen, J. Woerdman: Opt. Commun., **112**, 321 (1994)
13. W.-H. Lee, Prog. Optics **XVI**, 119 (1978)
14. C. Creath: In *Temporal Phase Measurement Methods in Interferogram Analysis*, ed. by D. Robinson, G. Reid (Inst. of Physics, Bristol 1993) 94–140